Tribology and Materials
Vol. 5, No. 1, 2026, pp. 38-49

ISSN 2812-9717
https://doi.org/10.46793/tribomat.2026.006

Combined mechanical mixing and hydrothermal synthesis of gehlenite-based ceramics

Auns Qusai Hashim AL-NEAMI [1,*], Hasnaa Shareef Ahmed JOLAK [1], Ayad Murad TAKHAKH [1], Fadhil Kareem FARHAN [2]

[1] College of Engineering, Al-Nahrain University, Baghdad, Iraq
[2] College of Science, Al-Karkh University of Science, Baghdad, Iraq
*Corresponding author: auns.q.hashim@nahrainuniv.edu.iq

Keywords

gehlenite
hydrothermal
mechanical mixing
sintering temperature
ceramics

History

Received: 12-09-2025
Revised: 10-12-2025
Accepted: 28-12-2025

Abstract

Gehlenite-based ceramics in the CaO-Al_2O_3-SiO_2 calcium aluminosilicate (CAS) system were synthesised using a combined approach that integrates hydrothermal treatment with mechanical mixing. Three formulations with varying $CaO:Al_2O_3:SiO_2$ ratios were prepared to investigate phase development. The precursor powders were first mechanically mixed in water and subjected to hydrothermal reaction at 200 °C for 48 h, then calcined (1000 °C) and sintered (1200 – 1250 °C) into dense pellets. X-ray diffraction (XRD) analysis confirmed the formation of gehlenite ($Ca_2Al_2SiO_7$) as the major phase, with minor secondary phases (wollastonite, corundum and cristobalite) noticeable at 1200 °C. Notably, at 1250 °C, the gehlenite reflections intensified, indicating more complete crystallisation. Scanning electron microscopy (SEM) revealed a fine microstructure of submicron particles (0.4 – 0.8 μm) agglomerated into a porous network. Energy-dispersive X-ray spectroscopy (EDS) showed elemental compositions in close agreement with the nominal stoichiometry (within approximately 3 wt. % for Ca, Al and Si), confirming homogeneous mixing. The combined hydrothermal-mechanical route produced gehlenite ceramics at a sintering temperature (approximately 1250 °C) lower than conventional solid-state methods, achieving high phase purity and uniform microstructure. The enhanced phase formation is attributed to improved precursor reactivity and nucleation from the hydrothermal step. This approach offers a viable pathway to fabricate CAS engineering ceramics with controlled crystallinity and porosity for potential high-temperature and structural applications.

1. Introduction

Calcium aluminosilicate (CAS) glass and ceramic systems are valued for their mechanical strength, thermal stability and optical properties, making them important in various industries [1]. Gehlenite ($Ca_2Al_2SiO_7$) is a melilite-phase ceramic that often appears in high-temperature processes and products. For example, gehlenite is commonly found in industrial waste residues, such as coal fly ash and metallurgical slags [2,3], and it occurs in many ceramic materials, including cements, ceramic tiles, porcelain glazes and even cookware glazes [2,4]. Gehlenite-based glass fibres have also been developed as biosoluble alternatives to traditional refractory ceramic fibres [5,6]. These broad applications highlight gehlenite's significance as an engineering material.

Understanding the CaO-Al_2O_3-SiO_2 ternary phase diagram is essential for tailoring the processing conditions of CAS ceramics [7]. Prior studies have provided phase diagram data for CAS systems and methods to predict phase formation in multicomponent systems [8,9]. The choice of firing temperature and cooling schedule significantly affects which phases (gehlenite or others) crystallise and with what microstructure. Typically,

synthesising crystalline gehlenite via conventional solid-state reactions requires high temperatures (approximately 1300 °C or higher) and can result in residual glassy phases if the temperature or soak time is insufficient [10,11]. Reducing the required sintering temperature while achieving complete crystallisation is a key challenge in CAS ceramics.

Several approaches have been explored to produce gehlenite-based materials, i.e. sol-gel and hydrothermal methods. Previous studies have shown that hydrothermal pretreatment can promote nucleation in CaO-Al_2O_3-SiO_2 precursors, leading to the formation of porous gehlenite ceramics upon subsequent firing. Adamczyk et al. [12] reported that hydrothermal activation of CaO-Al_2O_3-SiO_2 systems enhances gehlenite formation by facilitating early-stage nucleation processes. Similar effects of hydrothermal activation and controlled porosity development in CAS-based ceramic materials have also been noticed by Luo et al. [13] and Yang et al. [14]. Gehlenite exhibited significant volume expansion during sintering due to in-situ pore formation, which was achievable only after a hydrothermal step [15,16].

For solid-state reactions, the formation of gehlenite from kaolinite-calcium carbonate mixtures has been widely investigated in CaO-Al_2O_3-SiO_2 systems. Previous studies have reported the sequence of phase evolution, including the formation of intermediate anorthite, and emphasised the role of composition on phase development. Predictive approaches for phase formation in multicomponent ceramic systems have also been established [17,18]. Ke et al. [19] showed that varying CaO sources (like dolomite or wollastonite) in ceramic batches alters the phase assemblage in anorthite-gehlenite porcelains. These studies underline that precursor homogeneity and composition are critical to obtaining pure gehlenite.

Gehlenite-based materials are now being investigated for advanced applications such as biomedical implants and functional coatings. For instance, gehlenite has demonstrated bioactivity comparable to hydroxyapatite in bone tissue engineering scaffolds [20]. Electrospun composite nanofibers containing gehlenite nanoparticles showed enhanced osteoblast cell attachment and differentiation, indicating promise for bone regeneration applications [20,21]. Additionally, the melilite crystal structure of gehlenite can accommodate various dopants. Rare-earth-doped analogues (e.g. Ce^{3+}-doped $Ca_2Al_2SiO_7$ and Sm^{3+}/Eu^{3+}-doped $Ca_2Al_2SiO_7$ phosphors) exhibit luminescence properties that are explored for optical applications such as solid-state lighting and persistent phosphors [22,23].

Despite this progress, a clear research gap remains. Traditional solid-state sintering of gehlenite often requires high energy input (high temperatures for long durations) and may yield incomplete crystallisation or heterogeneous microstructures [10,11]. On the other hand, purely hydrothermal syntheses operate at much lower temperatures, but typically produce fine powders or require subsequent calcination to achieve crystallinity [13]. The novelty of the present work lies in combining hydrothermal treatment with mechanical mixing to take advantages of both methods. Mechanical mixing (including a mild mechanical activation) ensures uniform dispersion of reactants, while hydrothermal processing at 200 °C initiates low-temperature reactions and seed crystallite formation. It is hypothesised that this combined route will promote earlier nucleation of the gehlenite phase and thereby reduce the temperature needed for full crystallisation, compared to a purely mechanical route. By comparing three composition variants and multiple processing routes, this work aims to demonstrate a more energy-efficient and effective synthesis for gehlenite-based ceramics.

2. Materials and experimental methods

2.1 Materials

Analytical grade oxide powders were used as starting materials. Calcium oxide (CaO, 90 % purity, approximately 45 µm particle size, Loba Chemie), aluminium oxide (Al_2O_3, 99.73 % purity, approximately 50 µm particle size, Alfa Aesar) and silicon oxide (SiO_2, 99% purity, approximately 50 µm particle size, Thomas Baker) were obtained as dry powders. These raw materials were chosen to provide the necessary Ca, Al and Si sources for gehlenite ($Ca_2Al_2SiO_7$) formation. Three different compositions (samples) were formulated (labelled S1, S2 and S3) by varying the weight fractions of CaO, Al_2O_3 and SiO_2, as listed in Table 1.

Each 20 g batch was weighed according to the target stoichiometry. Sample S2 corresponds to the exact stoichiometric ratio for gehlenite (2 CaO : 1 Al_2O_3 : 1 SiO_2 in moles, which is 41 % CaO, 37 % Al_2O_3, 22 % SiO_2 by weight. Sample S1 has a higher Al_2O_3 content (Al-rich), while sample S3 has a higher SiO_2 content (Si-rich) relative to sample

Table 1. Compositions of prepared samples and their reference phase data

Sample	Composition, wt. %	Target phase (formula)	Estimated melting temperature, °C	Approximate sintering onset, °C
S1 (Al-rich)	30 CaO – 54 Al_2O_3 – 16 SiO_2	$CaAl_2Si_2O_{10}$ (close to anorthite)	2165	1624
S2 (stoichiometric)	41 CaO – 37 Al_2O_3 – 22 SiO_2	$Ca_2Al_2SiO_7$ (gehlenite)	2207	1655
S3 (Si-rich)	34 CaO – 30 Al_2O_3 – 36 SiO_2	$Ca_2Al_2SiO_9$ (silica-rich CAS)	2119	1590

S2. This allows exploration of the effect of slight off-stoichiometry on phase formation (excess alumina could lead to residual corundum, while excess silica might form wollastonite or cristobalite, as will be discussed).

Table 1 also shows the estimated melting and sintering temperatures for each composition, derived from the CAS phase diagram [8]. The melting points (2119 – 2207 °C) represent the theoretical liquidus temperature where each composition would fully melt, whereas the sintering temperature listed (1589 – 1655 °C) is an approximate temperature at which significant solid-state sintering or primary crystallisation would occur for that composition. It should be noted that actual firing temperatures (1200 – 1250 °C) are well below these theoretical values, so only partial fusion or solid-state reactions are expected in experiments.

2.2 Synthesis procedures

The flowchart in Figure 1 summarises the synthesis route for the combined hydrothermal–mechanical process. For each sample (S1, S2 and S3), the weighed powders were first mechanically mixed in deionised water to ensure uniform dispersion. Specifically, approximately 10 ml of deionised water was added to the powder mixture in a beaker, and the suspension was stirred vigorously using a magnetic stirrer for 3 h. This step (often termed a sol-gel or coprecipitation approach when precursors dissolve) helps to intimately blend the reactants and initiate any slight hydrolysis (for example, CaO may form $Ca(OH)_2$ in water). After mixing, the slurry for each sample was transferred to a stainless steel autoclave (hydrothermal reactor). The autoclave was sealed and heated at 200 °C for 48 h. Under

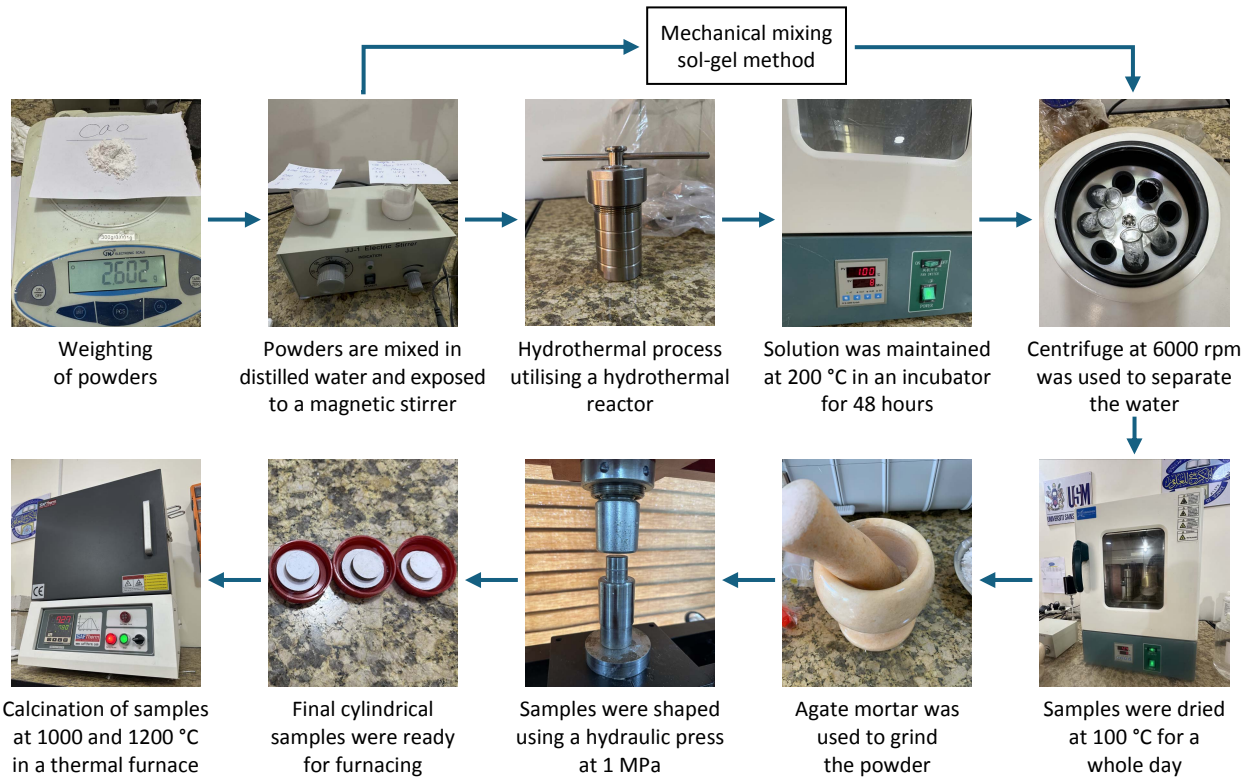

Figure 1. Schematic of the processing route combining mechanical mixing and hydrothermal treatment

these hydrothermal conditions (high temperature and autogenous vapour pressure), the mixed precursors can undergo chemical reactions or *in situ* crystallisation. This treatment is expected to produce fine-grained intermediate compounds (such as calcium silicate hydrates or aluminosilicate hydrates), which could act as low-temperature nuclei for gehlenite upon later firing.

After 48 h, the autoclaves naturally cooled to room temperature. The solid products (for each sample) were separated from the remaining liquid by decanting and centrifugation. The recovered solids were washed with distilled water and dried in a furnace at 100 °C for 24 h. This yielded dry powders that appeared finer and less agglomerated than the initial raw materials (a qualitative observation). These powders were then calcined at 1000 °C for 6 h in air (heating rate 5 °C/min) to decompose any hydroxides or gel-like species and to encourage preliminary oxide formation. Calcination was performed in alumina crucibles. After calcination, the furnace was allowed to cool slowly to room temperature. The calcined powders were gently ground in an agate mortar and pestle to break up any agglomerates and to restore a uniform fine powder.

The powders were next formed into pellets using uniaxial pressing. Approximately 20 g of each powder mixture was placed in a 20 mm-diameter steel die and pressed under a hydraulic press at 1 MPa. This forming step produced cylindrical green compacts with a diameter of approximately 20 mm and a thickness of approximately 4 mm. A pressure of 1 MPa was sufficient to form cohesive pellets for handling, although higher pressures can yield higher green densities. The pellets were somewhat porous in the green state, which is acceptable since significant densification was not a primary goal.

Finally, the pressed samples were sintered in a high-temperature furnace to induce the formation of crystalline phases. Sintering was carried out in air with a two-step schedule: heating at 5 °C/min to the target temperature, holding for 6 h and furnace cooling. Two different sintering temperatures were employed: 1200 and 1250 °C. The 1200 °C temperature is representative of a typical solid-state reaction temperature for gehlenite formation, while 1250 °C was used to examine if a modest increase would significantly improve phase purity. In practice, all hydrothermally treated samples (combined route) were sintered at 1250 °C to fully exploit the benefit of the precursor. Additionally, other samples (including those made without the hydrothermal step, described below) were sintered at 1200 °C for comparison. The rationale for choosing 1250 °C (which is still much lower than the materials' melting points) was to approach the reported threshold where gehlenite becomes the predominant phase [24], yet remain within a range accessible for standard furnace equipment and below the theoretical sintering onset (approximately 1600 °C, Table 1).

For comparison, a set of samples (SM1, SM2 and SM3) was prepared using a conventional route that consists only of mechanical mixing, without a hydrothermal step. In this route, the same raw materials and compositions were used. The powders were thoroughly mixed by grinding together in an agate mortar (dry mixing) for 30 min, followed by the addition of a small amount of ethanol and further grinding to simulate a slurry mixing (alternatively, they could be stirred in water for consistency; either way, the key difference is the absence of the autoclave treatment). The resulting mixtures were directly dried (if necessary) and then calcined at 1000 °C for 6 h, as in the combined process, to ensure a fair comparison after calcination. The calcined powders were pressed into pellets (1 MPa) to the same dimensions and sintered at 1200 °C for 6 h. This route, referred to as the mechanical mixing route, serves as a baseline for analysing the effect of hydrothermal pretreatment. By keeping all other parameters regarding the calcination, pressing, and sintering identical, any differences in phase content or microstructure can be attributed to the hydrothermal step.

2.3 Characterisation

Phase analysis was conducted on a Malvern Panalytical Aeris XRD diffractometer using a Cu Kα radiation source (λ = 1.5406 Å). X-ray diffraction (XRD) scans were collected over the 2θ range of 10 – 70°, at a step size of 0.02°. The diffraction patterns were identified against known JCPDS powder diffraction files for gehlenite and other possible phases. In particular, reflections near 2θ ≈ 31.3° and 2θ ≈ 27.0° were noted as characteristic of gehlenite. No full Rietveld quantification was performed. Instead, the relative peak intensities were used to qualitatively estimate phase fractions.

Scanning electron microscopy (SEM) from Thermo Fisher Scientific Axia ChemiSEM System

was used to examine the microstructure of sintered pellets. Fractured cross-sections of the sintered samples were mounted on stubs and coated with a thin carbon film to prevent charging under the electron beam. SEM images were acquired at an accelerating voltage of 15 kV. The average particle (grain) sizes were estimated by analysing SEM micrographs and performing image analysis across multiple areas. Energy-dispersive X-ray spectroscopy (EDS) was performed on selected areas of the SEM images to determine the elemental composition (Ca, Al and Si). The EDS system was calibrated with standards, and both atomic percent and weight percent of elements were obtained. To improve accuracy, the EDS analysis excluded the carbon peak (originating from the carbon coating) from the normalisation of oxygen and metal elements.

3. Results and discussion

3.1 Phase composition

The XRD characterisation of the synthesised ceramics provides clear evidence of gehlenite formation across all processing routes, with distinct differences in crystallinity and reaction completeness depending on the mixing method and sintering temperature. As illustrated in Figure 2, samples treated at 1200 °C, whether processed via the hydrothermal treatment combined with mechanical mixing approach or prepared by conventional mechanical mixing, exhibit gehlenite ($Ca_2Al_2SiO_7$) as the dominant crystalline phase, identified by its most intense diffraction peak at 2θ ≈ 31.3° along with a secondary prominent reflection near 2θ ≈ 27° [24], characteristic of the (211) and (002) gehlenite lattice planes. The appearance of these reflections at relatively moderate temperatures confirms the effectiveness of the adopted synthesis route in promoting early-stage gehlenite crystallisation. However, a closer comparison reveals that hydrothermally treated samples exhibit markedly sharper and higher-intensity gehlenite peaks, indicative of improved crystallinity and accelerated phase development relative to mechanically mixed samples, which show broader peaks and enhanced secondary phase signatures. These differences highlight the beneficial role of the hydrothermal step, which likely facilitates the formation of finely dispersed calcium aluminosilicate precursor species, enabling more efficient solid-state diffusion and nucleation, consistent with nucleation-controlled reaction pathways reported by Rietveld [9].

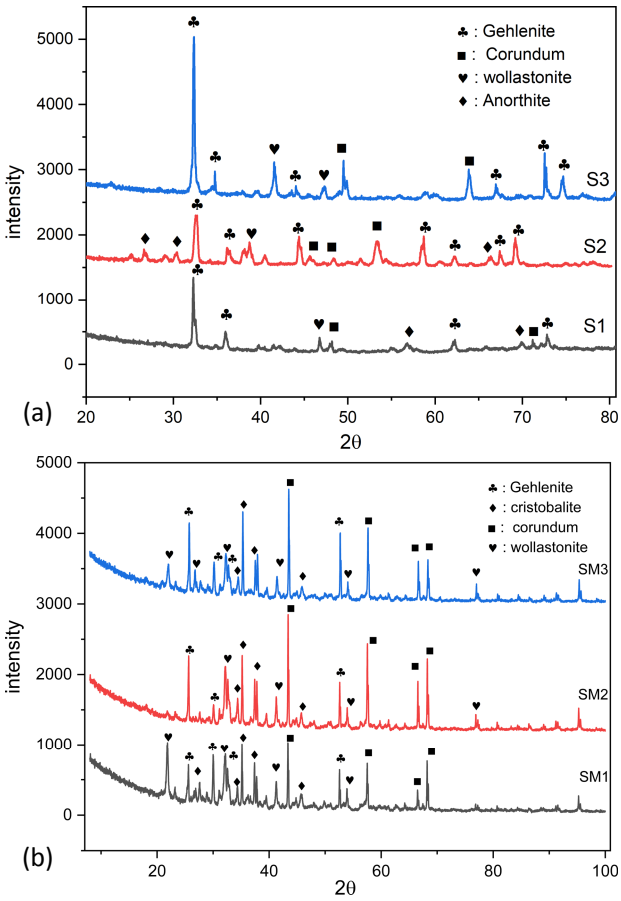

Figure 2. XRD patterns of samples fabricated at a sintering temperature of 1200 °C with: (a) hydrothermal treatment combined with mechanical mixing and (b) mechanical mixing

Secondary phases, including wollastonite (β-$CaSiO_3$), corundum (α-Al_2O_3) and cristobalite (SiO_2), appear in quantities consistent with compositional deviations in the CaO-Al_2O_3-SiO_2 system [19], with Al-rich sample (S1) retaining unreacted Al_2O_3, Si-rich sample (S3) presenting excess SiO_2 and $CaSiO_3$ and near-stoichiometric sample (S2) showing minimal impurities in accordance with thermodynamic predictions for the gehlenite stoichiometry [20]. The combined route significantly suppresses the intensity of these secondary reflections at 1200 °C, indicating more complete reaction progress and enhanced incorporation of excess oxide species into intermediate or target phases.

This remark aligns with literature reports demonstrating substantial improvements in gehlenite crystallinity and yield within the 1200 – 1300 °C range [10,15]. Notably, the samples fabricated with the combined method achieve this level of phase purity after a 6 h dwell at 1250 °C

(Fig. 3), suggesting that the hydrothermal step not only enhances low-temperature reactivity but also creates a precursor microstructure with shorter diffusion pathways, enabling more complete solid-state transformation during high-temperature treatment. These results collectively demonstrate the superior phase development achieved through the combined process, underscoring its value for preparing highly crystalline gehlenite ceramics at reduced processing temperatures.

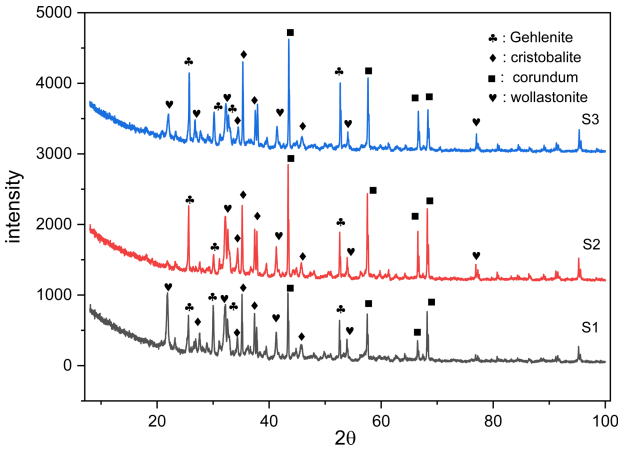

Figure 3. XRD patterns of samples fabricated at a sintering temperature of 1250 °C with hydrothermal treatment combined with mechanical mixing

3.2 Microstructure and chemical composition

The microstructures of the sintered samples, analysed with SEM, reveal important features influenced by both composition and processing route. Figures 4, 5 and 6 correspond to SEM images of sintered samples S1, S2 and S3, respectively, prepared by the combined hydrothermal-mechanical method (sintered at 1250 °C). All three samples show a porous ceramic microstructure with evidence of agglomerated fine grains. The grains are mostly submicron in size, measuring a few hundred nanometers. For example, Figure 4 (sample S1) shows clusters of particles of sizes ranging approximately from 0.45 to 0.79 µm. These grains appear to have necked together, forming an open porous network. There are visible voids or pores between the clusters, confirming that the material did not fully densify during sintering, likely due to the gehlenite phase's self-porosity phenomenon. Indeed, sample S1 (which had excess Al_2O_3) might have undergone a slight expansion upon sintering. This could be related to the mechanism reported by Yang et al. [14] and Jia et al. [15] for gehlenite, in which gas evolution (possibly due to the decomposition of residual hydroxides or carbonates) causes foaming. The analysis of a sponge-like structure in sample S1 is consistent with that, i.e. it exhibited "intriguing" volume growth during firing, resulting in macro- and mesopores throughout.

Figure 5 shows a somewhat different morphology of the stoichiometric gehlenite sample (sample S2). The particles in sample S2 appear slightly more sintered together, the grain size is a bit larger on average (many grains in the 0.5 – 1 µm range), and the pore spaces between grains are smaller compared to sample S1. This suggests that sample S2 underwent more effective sintering (partial densification), which makes sense because it had the highest fraction of liquid-phase formation at 1250 °C (gehlenite can form a transient liquid or sinter more readily when the composition is balanced). The microstructure of sample S2 is still generally porous, but it may have higher mechanical strength than sample S1 due to stronger grain bonding. The pore self-forming ability of gehlenite is still evident (as not all porosity is eliminated), aligning with previous findings that gehlenite ceramics maintain significant porosity across a wide temperature range [24,25]. It was noted that any slight glassy phase that might form at grain boundaries could also influence the microstructure, but EDS analysis suggests minimal glass in sample S2.

Figure 6 displays the microstructure of the Si-rich sample (sample S3). It shows fine grains similar to those in samples S1 and S2, but one distinguishing feature is the presence of larger, faceted particles scattered throughout the matrix. These could be residual silica (cristobalite) or wollastonite crystals that did not fully dissolve into the gehlenite matrix. The faceted nature (crystallites of 1 – 2 µm are noticed) and morphology suggest β-wollastonite, which often forms lath-like crystals. Surrounding these are much smaller particles (0.2 – 0.5 µm), which likely constitute the gehlenite matrix. As a result, the microstructure of sample S3 is a mix of very fine gehlenite grains and a few coarser second-phase crystals. The overall porosity of sample S3 is comparable to that of sample S2, i.e. pores of a few microns are visible, indicating that, although it is sintered, it also retains a lightweight structure. If these second-phase inclusions are eliminated (e.g. by adjusting composition or adding flux), the microstructure might become more uniform. However, in the case of sample S3, the effect of starting with surplus SiO_2 is demonstrated.

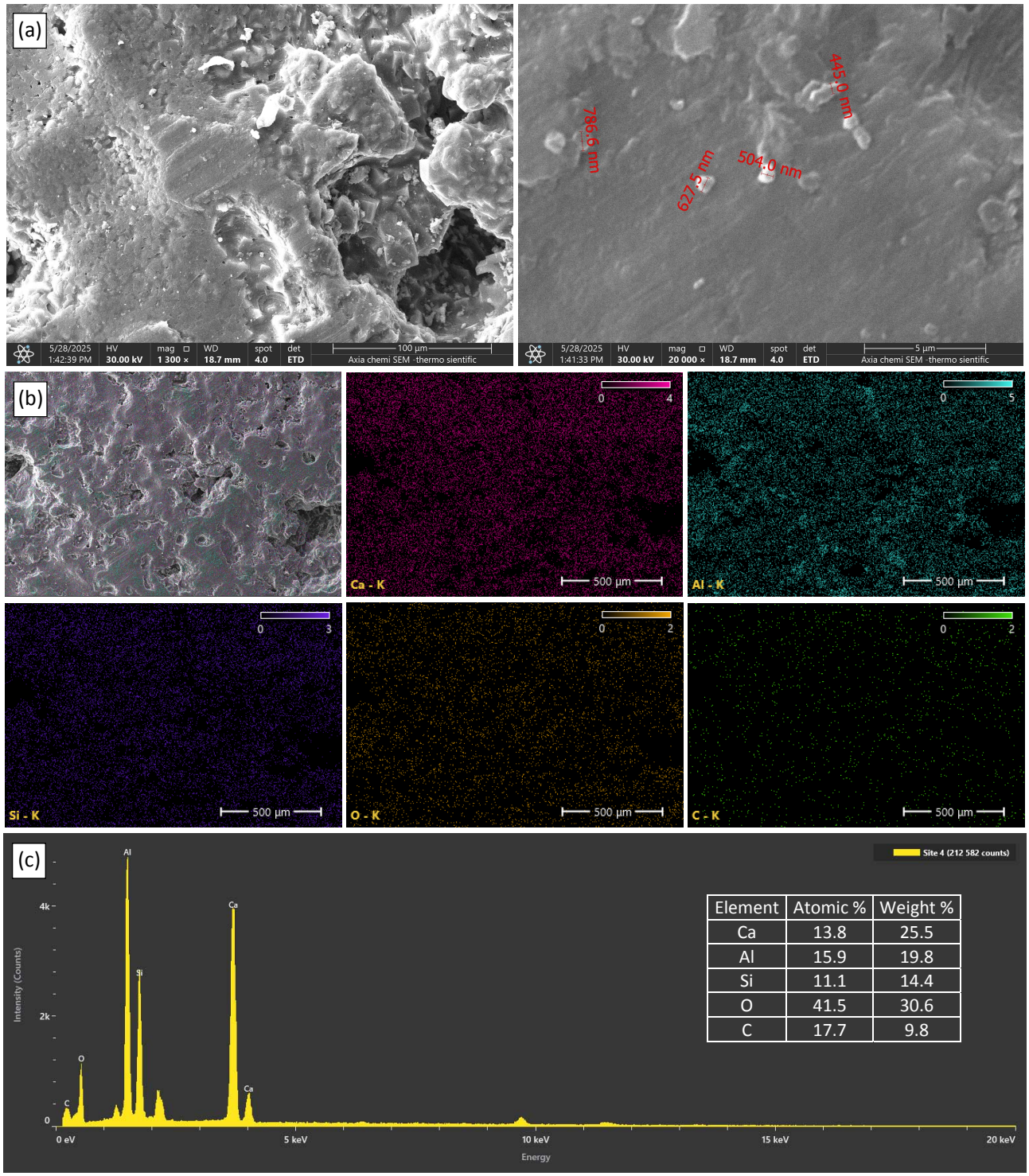

Element	Atomic %	Weight %
Ca	13.8	25.5
Al	15.9	19.8
Si	11.1	14.4
O	41.5	30.6
C	17.7	9.8

Figure 4. Sample S1: (a) SEM micrographs, (b) EDS elemental mapping and (c) EDS analysis

In all samples, the combined processing route produced very fine and homogeneously distributed grains. No evidence of large unreacted starting particles was noticed at the examined scale. Notably, features expected for unreacted CaO or Al_2O_3 (typically on the order of tens of micrometers) were absent, suggesting that these components were effectively consumed during processing. This finding highlights the effectiveness of the hydrothermal step in promoting the breakdown, redistribution and reaction of the raw materials, leading to improved microstructural uniformity after sintering at 1200 °C.

To facilitate comparison between samples, oxide compositions were estimated from the EDS elemental data using a stoichiometric normalisation approach. In this method, the measured cation weight percentages (Ca, Al and Si) obtained by EDS analysis were first renormalised after excluding contributions from carbon (conductive coating)

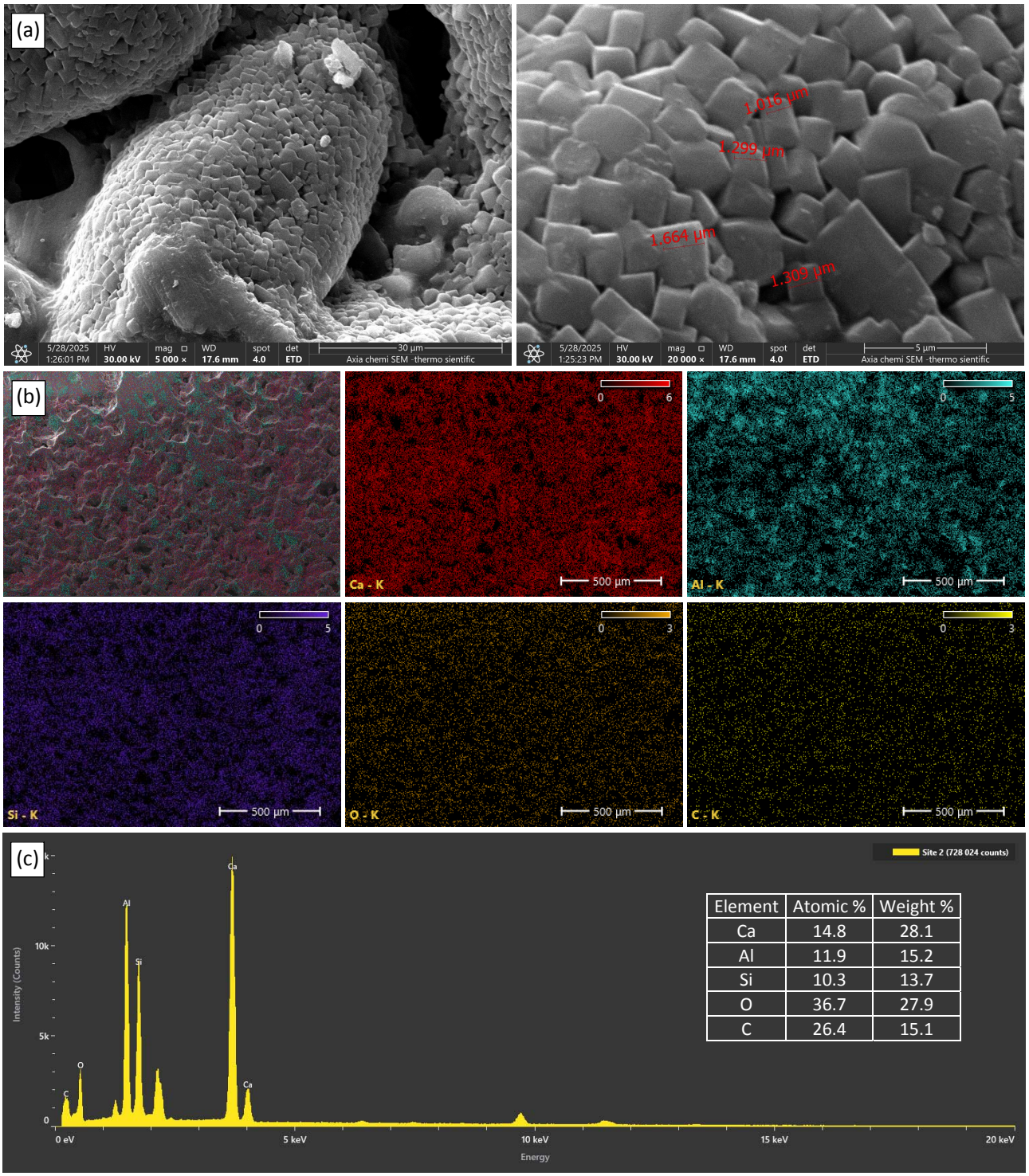

Element	Atomic %	Weight %
Ca	14.8	28.1
Al	11.9	15.2
Si	10.3	13.7
O	36.7	27.9
C	26.4	15.1

Figure 5. Sample S2 (a) SEM micrographs, (b) EDS elemental mapping and (c) EDS analysis

and oxygen, which is known to be quantified with limited accuracy in EDS measurements. The renormalised cation concentrations were then converted to their corresponding oxide forms (CaO, Al_2O_3 and SiO_2) using charge-balanced stoichiometry and molar-mass relationships, followed by normalisation to 100 wt. %. Owing to the semi-quantitative nature of EDS and the sensitivity of oxide back-calculation to small uncertainties in elemental quantification, the resulting oxide proportions should be regarded as approximate and are intended for comparative purposes only, rather than precise compositional determination [26-28].

EDS analysis was first performed on the Al-rich sample S1 (Fig. 4c) to assess the extent of aluminium enrichment relative to the stoichiometric composition. The elemental concentrations obtained from representative analysis areas show a pronounced increase in Al relative to Ca and Si, consistent with the intended

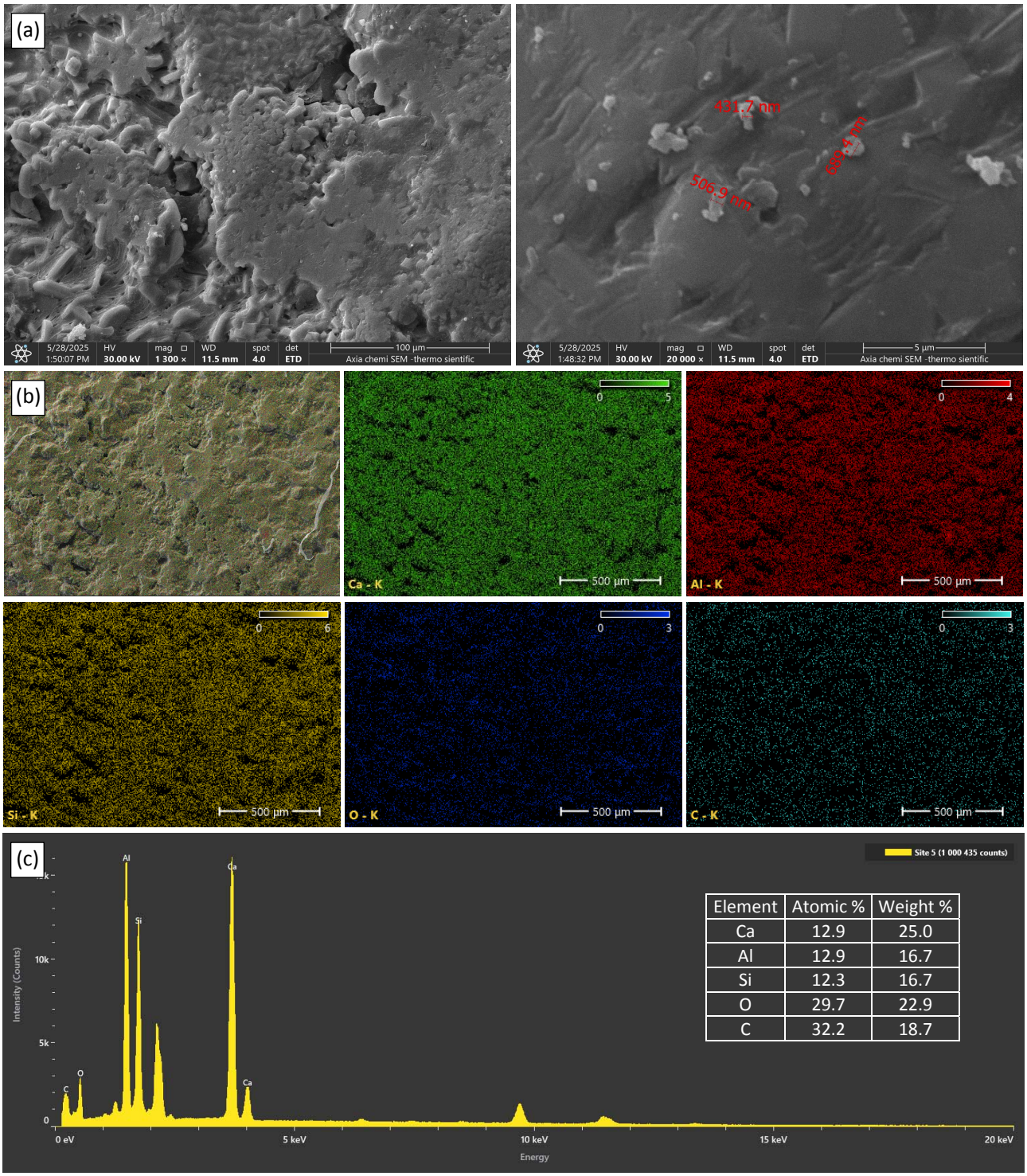

Element	Atomic %	Weight %
Ca	12.9	25.0
Al	12.9	16.7
Si	12.3	16.7
O	29.7	22.9
C	32.2	18.7

Figure 6 Sample S3 (a) SEM micrographs, (b) EDS elemental mapping and (c) EDS analysis

batch design. Applying stoichiometric normalisation to the EDS cation weight percentages (Ca, Al and Si) yields estimated oxide proportions of CaO ≈ 34.3 wt. %, Al_2O_3 ≈ 36.0 wt. % and SiO_2 ≈ 29.7 wt. %. These oxide values were not directly measured by EDS. They were calculated from elemental concentrations and should therefore be regarded as approximate, given the semi-quantitative nature of the technique and uncertainties associated with oxygen quantification and carbon coating effects. The estimated oxide proportions are in reasonable agreement with the nominal composition of sample S1 (30 wt. % CaO, 54 wt. % Al_2O_3 and 16 wt. % SiO_2), with deviations attributed to local compositional heterogeneity, as the analysed region may contain a higher fraction of gehlenite relative to residual Al_2O_3-rich regions. Such heterogeneity and phase coexistence are commonly noticed in Al-rich CaO-Al_2O_3-SiO_2 ceramics.

For comparison, EDS analysis was next conducted on the stoichiometric sample S2 (Fig. 5c) over a representative area spanning multiple grains. The averaged atomic concentrations of Ca ≈ 15 at. %, Al ≈ 12 at. % and Si ≈ 10 at. % yield a Ca : Al : Si ratio that closely approaches the expected 2 : 2 : 1 stoichiometry of $Ca_2Al_2SiO_7$ when normalised to the cation sublattice. Stoichiometric normalisation of the EDS cation weight percentages gives estimated oxide proportions of CaO ≈ 40.4 wt. %, Al_2O_3 ≈ 29.5 wt. % and SiO_2 ≈ 30.1 wt. %. In addition, the theoretical oxide proportions for ideal $Ca_2Al_2SiO_7$ are CaO = 40.9 wt. %, Al_2O_3 = 37.2 wt. % and SiO_2 = 21.9 wt. %. The differences between the EDS-derived estimates and the theoretical values are attributed to the semi-quantitative nature of EDS and minor biases in elemental quantification, particularly for Al and O. No systematic deviation from the intended stoichiometry is noticed, indicating that the processing route preserved the designed composition. These results provide compositional support for the predominantly single-phase gehlenite structure identified by XRD.

Finally, EDS analysis of the Si-rich sample S3 (Fig. 6c) was performed to evaluate the extent of silica enrichment relative to the stoichiometric composition. The elemental concentrations obtained from representative regions show elevated Si levels relative to Ca and Al, consistent with the intended batch formulation. Stoichiometric normalisation of the EDS cation data yields estimated oxide proportions of CaO ≈ 34.2 wt. %, Al_2O_3 ≈ 30.9 wt. % and SiO_2 ≈ 34.9 wt. %. As for samples S1 and S2, these oxide values were not directly measured but were calculated from elemental concentrations and should be regarded as approximate. The estimated oxide proportions are in good agreement with the nominal composition of sample S3 (34 wt. % CaO, 30 wt. % Al_2O_3 and 36 wt. % SiO_2), with deviations well within the expected experimental uncertainty. The EDS results, therefore, qualitatively confirm that sample S3 retained the intended Si-rich CaO-Al_2O_3-SiO_2 composition, consistent with the phase assemblage noticed by XRD.

Overall, the EDS data in wt. % provides strong evidence that the combined process achieved uniform elemental mixing. Each sintered sample's composition closely matches the target, meaning there was no significant leaching of elements during hydrothermal processing and no volatilisation during firing. The fact that EDS finds the elements in the correct ratio also implies high compositional accuracy of the synthesis. Essentially, the combined route produced what was intended, validating the method's precision. This addresses the question of "compositional accuracy" that might be raised by comparing the EDS results of samples S1, S2 and S3 with their nominal values, demonstrating that the process reliably reproduces the different chemistries. For instance, high accuracy in sample S2 shows that the approach can achieve the desired stoichiometry, and samples S1 and S3 show that it can intentionally vary Al or Si content and still recover those differences in the final product.

From a microstructural perspective, one intriguing outcome is the porosity present in these ceramics. Rather than achieving full density, the samples retained 20 – 40 % open porosity (as roughly estimated from image analysis of SEM micrographs). This is not necessarily a drawback. In fact, porous gehlenite could be useful for certain engineering applications (e.g. as an insulating material or a scaffold for composites). The cause of this porosity is twofold: (1) the relatively low sintering temperature (1250 °C is not enough to fully densify CAS ceramics, whose sintering onset is approximately 1600 °C) and (2) the evolution of gases or volume expansion from the hydrothermal-derived precursors.

The hydrothermal step likely introduced chemically bound water (as hydroxides) into the precursor. Upon calcination and sintering, dehydration and decomposition reactions can generate transient gases (H_2O and CO_2 if any carbonate forms) that can create bubbles. Additionally, gehlenite is known to exhibit a slight volume increase upon crystallisation from glass, which might contribute to pore generation [12-15]. Results support this, i.e. all samples, especially S1, had a foam-like microstructure with interconnected pores on the micron scale. This self-pore-forming behaviour is advantageous for making lightweight ceramics without the need for pore-formers. On the other hand, if a dense gehlenite ceramic is desired for structural purposes, it may need to be sintered at a higher temperature or subjected to hot-pressing to eliminate these pores.

4. Conclusions

This study demonstrates that a combined hydrothermal-mechanical synthesis route is an effective strategy for producing gehlenite ($Ca_2Al_2SiO_7$) ceramics with high phase purity,

improved homogeneity, and enhanced reactivity at relatively low sintering temperatures.

XRD results confirmed that gehlenite was the dominant phase in all samples, with those sintered at 1250 °C approaching single-phase composition and secondary phases present only in trace amounts. The hydrothermal pretreatment (200 °C, 48 h) significantly accelerated solid-state reactions by generating finely mixed precursor particles that facilitated nucleation, resulting in stronger gehlenite reflections and fewer than in only mechanically blended powders.

SEM analysis revealed a uniform fine-grained microstructure (approximately 0.5 µm grains) with approximately 30% open porosity and pore sizes of 1 to 5 µm, arising from the use of ultrafine powders and the nature of gehlenite crystallisation. EDS measurements confirmed that final compositions closely matched nominal Ca : Al : Si ratios, demonstrating reliable chemical accuracy and minimal contamination in the combined process.

The resulting porous gehlenite-rich ceramics show potential for high-temperature insulation, lightweight structures and composite preforms, while the reduced processing temperature and high phase purity suggest energy and cost benefits. Overall, this combined approach effectively bridges solution-based processing and conventional sintering, offering a versatile and potentially generalisable method for synthesising CAS and other multicomponent ceramics, with future work aimed at detailed phase quantification, mechanical property evaluation and optimisation of hydrothermal and sintering parameters.

Acknowledgement

We would like to express our sincere gratitude to Al-Nahrain University and Al-Karkh University of Science for their invaluable support and resources. Their academic environment has provided me with the necessary tools and inspiration to complete this work. We greatly appreciate the guidance and encouragement from the faculty members, and we are thankful for the opportunity to be a part of such esteemed institutions.

References

[1] J.F. Shackelford, R.H. Doremus (Eds.), Ceramic and Glass Materials, Springer, New York, 2008, DOI: 10.1007/978-0-387-73362-3

[2] S.V. Vassilev, C.G. Vassileva, A new approach for the classification of coal fly ashes based on their origin, composition, properties, and behaviour, Fuel, Vol. 86, No. 10-11, 2007, pp. 1490-1512, DOI: 10.1016/j.fuel.2006.11.020

[3] N.M. Piatak, M.B. Parsons, R.R. Seal II, Characteristics and environmental aspects of slag: A review, Applied Geochemistry, Vol. 57, 2015, pp. 236-266, DOI: 10.1016/j.apgeochem.2014.04.009

[4] W. Höland, G. Beall, Glass-Ceramic Technology, John Wiley & Sons, Hoboken, 2012.

[5] M. Rafienia, A. Bigham, A. Saudi, S. Rahmati, Gehlenite nanobioceramic: Sol-gel synthesis, characterization, and in vitro assessment of its bioactivity, Materials Letters, Vol. 225, 2018, pp. 89-92, DOI: 10.1016/j.matlet.2018.04.094

[6] H.G. Pfaender, Schott Guide to Glass, Springer, Dordrecht, 1996, DOI: 10.1007/978-94-011-0517-0

[7] E.M. Levin, C.R. Robbins, H.F. McMurdie, Phase Diagrams For Ceramists, The American Ceramic Society, Columbus, 1964.

[8] X. Lv, Z. Yan, High Temperature Physicochemical Properties of High Alumina Blast Furnace Slag, Springer, Singapore, 2022, DOI: 10.1007/978-981-19-3288-5

[9] H.M. Rietveld, A profile refinement method for nuclear and magnetic structures, Journal of Applied Crystallography, Vol. 2, No. 2, 1969, pp. 65-71, DOI: 10.1107/S0021889869006558

[10] P. Ptáček, T. Opravil, F. Šoukal, J. Havlica, R. Holešinský, Kinetics and mechanism of formation of gehlenite, Al-Si spinel and anorthite from the mixture of kaolinite and calcite, Solid State Sciences, Vol. 26, 2013, pp. 53-58, DOI: 10.1016/j.solidstatesciences.2013.09.014

[11] R.M. German, Sintering: From Empirical Observations to Scientific Principles, Butterworth-Heinemann, Waltham, 2014, DOI: 10.1016/C2012-0-00717-X

[12] Z. Adamczyk, B. Bialecka, M. Cempa, G. Majka, A. Polanska, Hydrothermal activation of fly ash from brown coal combustion, in Proceedings of the 18th International Multidisciplinary Scientific GeoConference (SGEM 2018), 02-08.07.2018, Albena, Bulgaria, pp. 83-90, DOI: 10.5593/sgem2018/1.4/S04.011

[13] H. Luo, Y. Wu, A. Zhao, A. Kumar, Y. Liu, B. Cao, E.-H. Yang, Hydrothermally synthesized porous materials from municipal solid waste incineration bottom ash and their interfacial interactions with chloroaromatic compounds, Journal of Cleaner Production, Vol. 162, 2017, pp. 411-419, DOI: 10.1016/j.jclepro.2017.06.082

[14] J. Yang, D. Li, Y. Fang, Synthesis of nanoscale CaO-Al_2O_3-SiO_2-H_2O and Na_2O-Al_2O_3-SiO_2-H_2O using the hydrothermal method and their characterization, Materials, Vol. 10, No. 7, 2017, Paper 695, DOI: 10.3390/ma10070695

[15] D. Jia, D. Kim, W.M. Kriven, Sintering behavior of gehlenite. Part I: Self-forming, macro-/mesoporous gehlenite – Pore-forming mechanism, microstructure, mechanical, and physical properties, Journal of the American Ceramic Society, Vol. 90, No. 6, 2007, pp. 1760-1773, DOI: 10.1111/j.1551-2916.2007.01704.x

[16] D. Jia, W.M. Kriven, Sintering behavior of gehlenite, Part II. Microstructure and mechanical properties, Journal of the American Ceramic Society, Vol. 90, No. 9, 2007, pp. 2766-2770, DOI: 10.1111/j.1551-2916.2007.01835.x

[17] M. Dondi, M. Raimondo, C. Zanelli, Clays and bodies for ceramic tiles: Reappraisal and technological classification, Applied Clay Science, Vol. 96, 2014, pp. 91-109, DOI: 10.1016/j.clay.2014.01.013

[18] I. Denry, J.A. Holloway, Ceramics for dental applications: A review, Materials, Vol. 3, No. 1, 2010, pp. 351-368, DOI: 10.3390/ma3010351

[19] S. Ke, X. Cheng, Y. Wang, Q. Wang, H. Wang, Dolomite, wollastonite and calcite as different CaO sources in anorthite-based porcelain, Ceramics International, Vol. 39, No. 5, 2013, pp. 4953-4960, DOI: 10.1016/j.ceramint.2012.11.091

[20] A. Bigham, S. Kermani, A. Saudi, A.H. Aghajanian, M. Rafienia, On the bioactivity and mechanical properties of gehlenite nanobioceramic: A comparative study, Journal of Medical Signals & Sensors, Vol. 10, No. 2, 2020, pp. 105-112, DOI: 10.4103/jmss.JMSS_41_19

[21] M.A. Baghbadorani, A. Bigham, M. Rafienia, H. Salehi, *In vitro* studies of polycaprolactone nanofibrous scaffolds containing novel gehlenite nanoparticles, Journal of Medical Signals & Sensors, Vol. 11, No. 2, 2021, pp. 131-137, DOI: 10.4103/jmss.JMSS_42_20

[22] L. Zhao, J. Mao, B. Jiang, X. Wei, M. Yin, Y. Chen, A new yellow long persistent luminescence phosphor $Ca_2Al_2SiO_7:Eu^{2+},Tm^{3+}$ found by co-doping Ln^{3+} (Ln = Ce, Pr, Nd, Sm, Gd, Tb, Dy, Ho, Er, Tm, Yb, Lu) with Eu^{2+} in $Ca2Al2SiO_7$ host, Journal of Luminescence, Vol. 206, 2019, pp. 6-10, DOI: 10.1016/j.jlumin.2018.10.038

[23] N. Kodama, T. Takahashi, M. Yamaga, Y. Tanii, J. Qiu, K. Hirao, Long-lasting phosphorescence in Ce^{3+}-doped $Ca_2Al_2SiO_7$ and $CaYAl_3O_7$ crystals, Applied Physics Letters, Vol. 75, No. 12, 1999, pp. 1715–1717, DOI: 10.1063/1.124799

[24] Y. Xu, P. Song, W. Cao, H. Li, J. Liang, Effect of Al_2O_3-SiO_2 addition on gehlenite growth and the mechanical performance of steel slag, Crystals, Vol. 11, No. 8, 2021, Paper 936, DOI: 10.3390/cryst11080936

[25] F. Zenikheri, A. Harabi, B. Boudaira, F. Bouzerara, A. Guechi, S.-E. Barama, L. Foughali, N. Karboua, Elaboration of porous gehlenite and anorthite based ceramics using low price raw materials, Cerâmica, Vol. 62, No. 363, 2016, pp. 242-248, DOI: 10.1590/0366-69132016623632005

[26] J.I. Goldstein, D.E. Newbury, J.R. Michael, N.W.M. Ritchie, J.H.J. Scott, D.C. Joy, Scanning Electron Microscopy and X-Ray Microanalysis, Springer, New York, 2018, DOI: 10.1007/978-1-4939-6676-9

[27] D.E. Newbury, N.W.M. Ritchie, Performing elemental microanalysis with high accuracy and high precision by scanning electron microscopy/silicon drift detector energy-dispersive X-ray spectrometry (SEM/SDD-EDS), Journal of Materials Science, Vol. 50, No. 2, 2015, pp. 493-518, DOI: 10.1007/s10853-014-8685-2

[28] S.J.B. Reed, Electron Microprobe Analysis and Scanning Electron Microscopy in Geology, Cambridge University Press, Cambridge, 2005, DOI: 10.1017/CBO9780511610561